 https://doi.org/10.3311/PPch.21815

Periodica Polytechnica Chemical Engineering, 67(3), pp. 490–503, 2023

The Effect of Operating Parameters on Total Cross-membrane Flux in a PVDF Flat Sheet Membrane

Hafsa Bekraoui[1,2*], Driss Nehari[2], Touhami Baki[3], Mouad Bousmaha[2]

[1] Laboratoire Structures Intelligentes, University of Ain Temouchent, P. O. B. 284, 46000 Ain Temouchent, Algeria
[2] Department of Mechanical Engineering, Faculty of Science and Technology, University of Ain Temouchent, P. O. B. 284, 46000 Ain Temouchent, Algeria
[3] Department of Mechanical Engineering, Faculty of Mechanical Engineering, University of Science and Technology of Oran Mohamed-Boudiaf, P. O. B. 1505, Bir El Djir 31000, Oran, Algeria
[*] Corresponding author, e-mail: hafsa.bekraoui@univ-temouchent.edu.dz

Received: 07 January 2023, Accepted: 24 April 2023, Published online: 20 July 2023

Abstract

Membrane distillation (MD) is an emerging thermal membrane technology that involves water vapor driven by a vapor pressure gradient over a hydrophobic membrane. MD faces several challenges, one of which is the flux of water vapor. The total cross-membrane flux in membrane distillation was investigated in this paper using the co-current PVDF flat sheet for direct contact membrane distillation applications. The goal of this research is to improve total cross-membrane flux. The effect of various operational parameters is studied, including feed inlet temperature (333.15–358.15 K), feed flow rate (1–2.5 kg/s), permeate inlet temperature (288.15–313.15 K), and feed inlet NaCl concentration (0.035 to 0.485 kg/kg). To acquire a good value of total cross-membrane flux, their interactions with the total cross-membrane flux are studied in this work. The obtained results were computed during MATLAB-Simulations under several scenarios adopting the Trial-&-Error approach. This last inputs various parameters' values and thus draws the required curves to be discussed and analyzed. The results indicated that the PVDF flat sheet membranes provide a significantly higher total cross-membrane flux at higher feed input temperatures, producing a 73.2075 kg/(m^2 h) at a feed inlet temperature of 358.15 K, a permeate inlet temperature of 293.15 K, and a flow rate of 2.5 kg/s, with a feed inlet NaCl concentration of 0.035 kg/kg. Feed inlet temperature significantly affected the total flux through the membrane; however, flow rate, permeate inlet temperature, and feed inlet NaCl concentration had a less significant effect.

Keywords

desalination process, permeate flux, direct contact membrane distillation (DCMD), operating parameters

1 Introduction

Water scarcity is more visible today than ever due to wasteful consumption, urbanization, and population growth (the world population has reached 7.9 billion people [1]. By 2050, approximately half of the world's population will confront water scarcity, according to UN predictions [2]. To resolve this shortage and satisfy people's needs, membrane distillation (MD) technology is one of several water treatment methods In the literature, such methods include:

1. reverse osmosis (RO) [3, 4],
2. ultrafiltration (UF) [5, 6],
3. ion exchange (IX) [7, 8],
4. coagulation and flocculation [9],
5. activated carbon filtration [10, 11]
6. chlorination [12],
7. ozonation [13].

These are some of the various water treatment procedures utilized alongside membrane distillation. For providing potable water around the world worldwide, MD is concerned with quantity and quality [14]. This technology has sparked much attention due to its low equipment cost, low energy usage, simple pretreatment, and achievable operation conditions. Because the process liquid does not need to be heated above its boiling temperature in this technology, the operating pressure and temperature are both reduced compared to alternative methods [15].

The MD is a developing water treatment membrane separation technique that involves water vapor driven by a vapor pressure gradient over a hydrophobic membrane [16]. This method combines thermal distillation and membrane separation using a hydrophobic porous

Cite this article as: Bekraoui, H., Nehari, D., Baki, T., Bousmaha, M. "The Effect of Operating Parameters on Total Cross-membrane Flux in a PVDF Flat Sheet Membrane", Periodica Polytechnica Chemical Engineering, 67(3), pp. 490–503, 2023. https://doi.org/10.3311/PPch.21815

membrane, which is a thin sheet or film of semipermeable material [17]. The resulting device separates liquid and gas phases and is designed to reject undesirable substances from the feed side, such as dissolved salts and mineral components (non-volatile particles). Instead, only water molecules in the vapor phase (volatile particles) are permitted to pass through the membrane toward the permeate side. As a necessity, the separation process consists of three significant steps:

1. The demand for thermal energy is reduced on the hot feed side between 318.15 and 363.15 K [18], and
2. through the hydrophobic membrane pore, diffusing volatile vapor molecules and migrating to the permeate side by a driven force, then
3. the condensation carrying between the permeate side and the bulk wall [19].

The MD process is grouped into four basic configurations based on the nature of the condensation operation; the permeated water vapor is condensed via various means. In all configurations where the heated liquid solution is in direct contact with a hydrophobic membrane to transfer as a vapor through it, the feed side of the membrane stays the same. The most straightforward MD configuration is direct contact membrane distillation (DCMD), which uses a heated liquid in direct contact with both membrane interfaces [20, 21].

Many studies have been interested in the enhancement of the permeate flux and the reduction of membrane fouling, such as the modification of pore size, by putting two geometric forms of 3D turbulence promoters (circular and square) into the feed channel between a hydrophobic composite membrane and an acrylic plate in a silicone rubber 1 mm thick while leaving the permeate channel empty. Chang et al. [22] aimed to prevent vibrations from increasing the membrane's stability and reducing the temperature polarization effect by increasing heat and mass transmission. Due to the significant temperature differential, Chang reached a higher value in the countercurrent flow, where the flow was increased by 61.7%. Much research, rather than membrane design, focuses on establishing optimum system configurations for maximum energy efficiency. Francis et al. [23] assessed the improvements of modified and innovative MD configuration designs, prioritizing upscaling impacts and pilot-scale research, reducing heat loss, and improving mass transmission to obtain a high flux. Suárez et al. [24] developed a mathematical model to predict distillate flux in DCMD when an inorganic fouling layer forms at the membrane surface due to salt deposition related to cake-filtration theory to represent the permeate flux drop once the fouling membrane begins. The obtained permeate flux is ~12 to 14 kg/(m^2 h) then decreases to zero once membrane fouling occurs. Hidayah et al. [25] have fabricated a polysulfone-nano zinc oxide (ZnO) membrane by mixing one wt% nano ZnO into 19 wt% polysulfones (PSFs) polymers with a 6000 Da polyethylene glycol (PEG) additive and 1 min ultraviolet (UV) irradiation, as pore former on the membrane structure to increase the stability and value of the permeate flux, and a three wt% of polyvinyl alcohol (PVA) coating to increase the rejection value.

Furthermore, Khalifa et al. [26] assessed experimentally and analytically the effect of the main parameters on the performance of the DCMD system, such as the feed temperature, which the researchers increased from 313.15 to 363.15 K with an increment of 283.15 K at five different permeate temperatures (278.15, 283.15, 288.15, 293.15, and 298.15 K). The permeate flux increased from 80 to 100 kg/(m^2 h), the permeate temperature varied from 278.15 to 298.15 K with an increment of 278.15 K at different feed temperatures (323.15, 343.15, and 363.15 K) with a feed salinity of 2 g/L. The permeate flux increased as the permeate temperature decreased, and the flow rate varied from 2.5 to 4.6 L/min. The permeate flux increased by 31% from 55 to 72 kg/(m^2 h), and feed concentration was tested at four levels: 0.14, 2, 43, and 100 g/L at a permeate temperature of 298.15 K. The permeate flux decreased continuously. Alwatban et al. [27] concentrated on analyzing the influence of properties and operational parameters on a three-dimensional DCMD system using a computational fluid dynamics (CFD) model. The researchers also used a net-type spacer in the feed and permeate channels to reduce the influence of polarization. Permeate flux improved by 50% from 32.31 to 59.05 kg/(m^2 h) at Reynolds number (Re) Re = 100 and Re = 1500, respectively, permeate flux generation increased with Reynolds number, and polarization was reduced by up to 30%. This result is consistent with the previous findings conducted by Laqbaqbi et al. [28]. They also investigated the fouling problem on both the membrane surface and within its pores while treating textile dye solutions with polyvinylidene fluoride (PVDF) flat sheet membranes. In addition, Al-Salmi et al. [29] investigated a DCMD module to generate water from an oil field using a polypropylene (PP) membrane with a 0.2 μm pore size. According to the findings, DCMD offers a strong potential for treating hypersaline oilfield water. The overall salt rejection rate was greater than 99.9%. By fluorinating zinc oxide (ZnO)

over an electrospun PVDF membrane, Li et al. [30] created a slipping super-hydrophobic nanofibrous composite (FZP) membrane with contact and sliding angles of 162.3° and 9.8°, respectively by fluorinating a ZnO-blend electrospun PVDF membrane. The findings were compared to those of neat and nanofibrous membrane (ZP); the membrane made from a PVDF membrane with ZnO added demonstrated strong anti-wetting performance, a high value of liquid entry pressure (LEP) while desalting NaCl solution, and a steady permeate flux. Foureaux et al. [31] used polytetrafluoroethylene (PTFE) and PVDF membranes to test DCMD for water reclamation for eight months. For a PTFE membrane with a spacer, the permeate flux was 6.82 L/(m^2 h). Both membranes maintained a 99.2% salt rejection rate. DCMD was identified by researchers as a prospective choice for performing MD for future water reclamation.

Moreover, Wanke et al. [32] also performed a mussel-inspired technique of addition by electrospinning a layer of polyvinylpyrrolidone-co-polymethyl methacrylate (PVP-co-PMMA) over a hydrophobic commercial PVDF microfiltration membrane modified with the polydopamine membrane. The inclusion of this layer with hydrophilic properties quadruples the permeate flux. Niknejad et al. [33] conducted an electro-blowing method to create a superhydrophobic nanofibrous polymethyl methacrylate (PMMA) membrane that outperformed commercial membranes such as polypropylene (PP) and polytetrafluoroethylene (PTFE) in terms of permeate flux. In both 35 and 150 g/L salty water desalination, the modified PMMA membrane outperformed commercial membranes. The PMMA membrane with the highest permeate flux achieved 41.04 and 35.94 kg/(m^2 h) due to its superhydrophobicity of 164.2° and high liquid entry pressure (LEP) of 227.3 kPa. PTFE and PP, on the other hand, gave a decent permeate flux of 35 kg/(m^2 h) The nanofibrous PMMA membrane is a promising choice for performing promising desalination using the DCMD method due to its high production rate, simplicity of fabrication, and cost-effectiveness. Also, Bin Bandar et al. [34] tested a modified membrane with well water as a feed stream and found an average permeate flux of 13.10 kg/(m^2 h) and salt rejection of 98.96%. Fortunato et al. [35] compared DCMD's efficiency in treating a synthetic textile dye solution to that of other research studies. Furthermore, it is important to note that the influence of operating parameters on DCMD performance in synthetic effluents, including reactive and dispersed dyes, was examined by de Sousa Silva et al. [36]. The performance of the DCMD improved with feed temperature and flow rate, allowing it to generate a permeate flux of 97.3% for reactive dyes and 98.7% for dispersed dyes while rejecting more than 98% of dyes.

Lastly, to facilitate global DCMD module scale-up for seawater desalination, Dong et al. [37] developed two open-source simulators of a flat sheet membrane in plate-and-frame configuration and a hollow fiber membrane to enable global DCMD module scale-up for seawater desalination. where the simulators used laboratory-scale experimental data from a single configuration as simulated inputs to predict the performance of scaled-up modules in co-current and counter-current configurations, as well as a shell- and bore-side feeds (for hollow fiber modules). A connected "tanks-in-series" and "black box" analysis approach was devised to create profiles of all essential DCMD parameters vs membrane length. The simulators developed were then used to predict the desalination performance of industrial-scale flat sheet and hollow fiber modules, as well as the effect of membrane physical properties, module dimensions, and operating conditions on the performance of large-scale DCMD modules.

The current work examines how to enhance the permeate water vapor flux by using a co-current PVDF flat sheet DCMD system by highlighting the operating parameters on permeate flux that Dong et al. [37] did not investigate via their numerical model, namely NaCl concentration, flow rate, and feed and permeate temperatures, pointing to the effect of the temperature and concentration polarization. This work aimed to compare the effects of different operating parameters on the permeate flux enhancement.

2 Theoretical model

This section describes the computational modeling work for DCMD transport processes in a flat sheet membrane proposed by Dong et al. [37].

2.1 Heat and mass transfer

The DCMD system couples both heat and mass transfer mechanisms, as shown in Fig. 1.

2.2 Mass tranfer

The hot feed solution concentration is described with the mass transfer. The general form of permeate flux J_w (kg/(m^2 h)) in the MD process, which crosses the pores of a hydrophobic membrane as water vapor, can be written as:

$$J_w = A \times C_m \times \left(P_{fm}^{sat} - P_{pm}^{sat} \right). \quad (1)$$

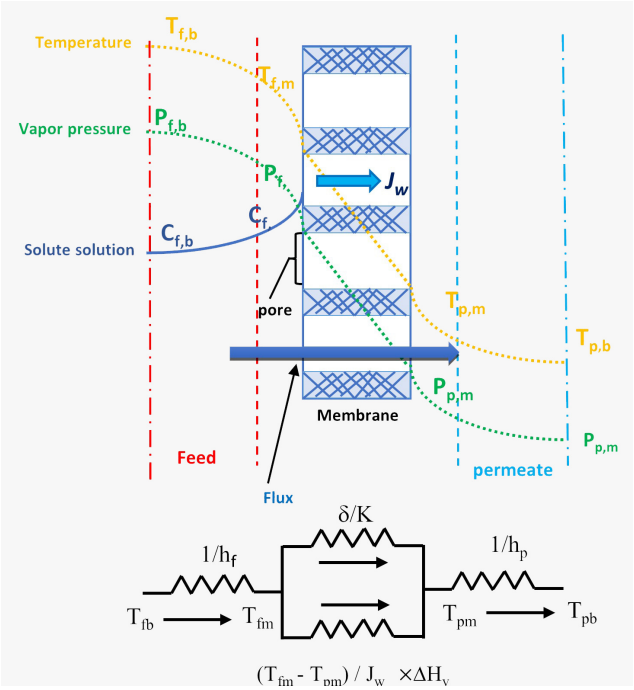

Fig. 1 Schematic of heat and mass transfer in the DCMD process with the variation of temperatures and concentrations

The surface area of the membrane (m^2) is A, C_m is the overall mass transfer coefficient (water vapor membrane permeability) (kg/(m^2 Pa s)), P_{fm}^{sat} is the saturation vapor pressure (Pa) at the feed-membrane interface, and P_{pm}^{sat} is the vapor pressure (Pa) at the permeate-membrane interface. The pure water vapor is expressed by the exponential relation between saturated vapor pressure and temperature according to Antoine's equation:

$$P = \exp\left(23.20 - \frac{3816.44}{T_m - 46.13}\right). \tag{2}$$

P is the vapor pressure in Pa, and T_m is the local temperature on the membrane surface in K. The feed side saturated water vapor pressure can be expressed as the function of the water activity coefficient (a_w), which varies with temperature and solute content, and could be determined using empirical equations (NRTL and VanLarr) or using experimental data using Raoul's law [26, 38–40]:

$$P_{fm}^{sat} = \left(1 - x_{\mathrm{NaCl}}\right) \times a_w \times P_w^{sat} \tag{3}$$

$$a_w = 1 - 0.5 \times x_{\mathrm{NaCl}} - 10 \times x_{\mathrm{NaCl}}^2 . \tag{4}$$

Where x_{NaCl} is the NaCl mole fraction in water solution, a_w is water activity, P_w^{sat} is the water vapor pressure feed-membrane (permeate-membrane interfaces from [41]):

$$\lg P^{sat} = A - \frac{D}{T + C} \tag{5}$$

$$p^{sat} = 133.322 \times 10^{\left\{8.07131 - \left[1730.630/(T - 39.724)\right]\right\}} . \tag{6}$$

Based on the mean temperature across the membrane surfaces, the Antoine equation is used, T_m, where:

$$T_m = \frac{T_{fm} + T_{pm}}{2} . \tag{7}$$

2.3 Heat transfer

Heat transfer occurs in three regions in the co-current flow DCMD module, referring to the DCMD configuration in Fig. 1, based on inlet and outlet temperature.

Convective heat transfer (W) in the feed solution side of the membrane, where fluid with such a high temperature and salinity is flowing along the surface, and Newton's law of cooling governs convective heat transfer (W) through the feed boundary layer between the feed side and the membrane surface, as shown in Eq. (8) [42]:

$$Q_f = h_f \times \left(T_{fb} - T_{fm}\right). \tag{8}$$

Where T_{fb} and T_{fm} is the bulk feed and membrane surface temperatures in (K), respectively, and h_f is the feed convective heat transfer coefficient (W/(m^2 K)) obtained using different correlations based on the regime type (laminar or turbulent).

Convective heat transfer (W) in the boundary layer region from membrane surface to permeate solution:

$$Q_p = h_p \times \left(T_{pm} - T_{pb}\right). \tag{9}$$

Where T_{pb} and T_{pm} are the bulk permeate and membrane surface temperatures on the permeate side, respectively, and h_p is the permeate convective heat transfer coefficient (W/(m^2 K)), determined using various correlations.

Heat transfer across the membrane (Q_m), as indicated in Eq. (10), through the conductive heat (Q_c) carried by the membrane material and through the pores by the latent heat (Q_v) carried by the water vapor diffusion, as shown in Eq. (11) and Eq. (13), respectively.

$$Q_m = Q_c + Q_v \tag{10}$$

Where the conductive heat Q_c calculated conduction Fourier's law calculates the conductive heat (Q_c) as:

$$Q_c = A \times h_m \times \left(T_{fm} - T_{pm}\right) = \frac{A \times K_m}{\delta} \times \left(T_{fm} - T_{pm}\right) . \tag{11}$$

Where δ is the thickness membrane (m), and K_m (W/(m K)) is the effective thermal conductivity of the membrane, can be calculated using the membrane material data:

$$K_m = (1-\varepsilon) K_s + \varepsilon K_g . \quad (12)$$

Where ε is the porosity, K_s and K_g are the thermal conductivity (W/(m K)) of solids and gas in pores. The evaporative heat transfer Q_v is the product between the vapor mass flux J_w (kg/(m^2 h)) and the water vaporization enthalpy ΔH_v (kJ/kg):

$$Q_v = J_w \times \Delta H_v . \quad (13)$$

The enthalpy of water vaporization (ΔH_v) (kJ/kg) is given as [26]

$$\Delta H_v = 1.75535 \times T_{fm} + 2024.3 . \quad (14)$$

Where T_{fm} is the feed membrane surface temperature in (K). According to Eq. (8) and Eq. (9), this heat flow must be equal to both the convective heat flux across the feed boundary layer (Q_f) and across the permeate boundary layer (Q_p) to validate the conservation of the energy. As a result, the heat balance is given in Eq. (15):

$$Q_f = Q_m = Q_p . \quad (15)$$

The membrane surface temperature at both the feed and the permeate side can be calculated as [43]:

$$T_{fm} = \frac{k_m \times \left(T_{pb} + \frac{h_f}{h_p} \times T_{fb} \right) + \left(\left(\delta \times \left(h_f \times T_{fb} - J_w \times \Delta H_v \right) \right) \right)}{\left(k_m \right) + \left(h_f \times \left(\delta + \left(\frac{k_m}{h_p} \right) \right) \right)} \quad (16)$$

$$T_{pm} = \frac{k_m \times \left(T_{fb} + \frac{h_p}{h_f} \times T_{pb} \right) + \left(\left(\delta \times \left(h_p \times T_{pb} + J_w \times \Delta H_v \right) \right) \right)}{\left(k_m \right) + \left(h_p \times \left(\delta + \left(\frac{k_m}{h_f} \right) \right) \right)} . \quad (17)$$

The convective heat transfer coefficient h can be determined using Eq. (18), which varies based on the MD module's operating conditions. This coefficient can be calculated by Eq. (18) (W/(m K)):

$$h = \frac{\mathrm{Nu} \times k}{D_h} . \quad (18)$$

Where k is the fluid's average thermal conductivity ((W/(m K)) on the feed and the permeate side, D_h is the flow channel's hydraulic diameter (m), and Nu is the dimensionless Nusselt number which is determined from the following correlations types and valid for flows in both the feed and the permeate sides:

- The case of the laminar channel flow (Re < 10^4):

$$\mathrm{Nu} = 0.664 \times \mathrm{Pr}^{1/3} \times \mathrm{Re}^{1/2} . \quad (19)$$

- In the case of the turbulent channel flow, Dittus Boelter correlation (Re > 10^4):

$$\mathrm{Nu} = 0.023 \times \mathrm{Re}^{0.8} \times \mathrm{Pr}^{0.4} . \quad (20)$$

Where Re is the Reynolds number of the channel flow, and Pr is the Prandtl number which is the ratio of viscous diffusion rate to thermal diffusion rate and is defined as:

$$\mathrm{Pr} = \frac{\mu \times c_p}{k} . \quad (21)$$

Where μ is the dynamic viscosity (Pa s), K is the thermal conductivity, and C_p is the fluid's specific heat (J/(kg K)). The total heat transfer in the membrane versus overall heat coefficient U (W/(m^2 K)) is determined as follows:

$$Q_m = U \times \left(T_{fb} - T_{pb} \right) . \quad (22)$$

Where this overall heat coefficient U can be calculated as:

$$U = \left[\frac{1}{h_f} + \frac{1}{\left(\frac{k_m}{\delta} \right) + \frac{J_w \times \Delta H_v}{\left(T_{fm} - T_{pm} \right)}} + \frac{1}{h_p} \right]^{-1} . \quad (23)$$

To solve the problem. The steady-state simulation algorithm was implemented using MATLAB code to simulate the states of mass and heat transport. The "Supporting Information" contains the "Function file" and the "MATLAB code main file" as a zip file and is available on the journal website.

3 Results and discussion

The effect of feed inlet temperature, permeate inlet temperature, flow rate, and feed inlet NaCl concentration on total cross-membrane flux will be studied and discussed in this section. The total cross-membrane flux expresses the permeate generated during membrane separation per unit of time and membrane area. The flux is expressed in kilograms per square meter per hour (kg/(m^2 h)). As described in Eq. (1). This is a significant character, and it is affected by operational settings. The total cross-membrane flux performance of a co-current PVDF flat sheet DCMD system is investigated at various feed inlet temperatures, permeate inlet temperatures, flow rates, and feed inlet NaCl concentrations.

3.1 Effect of feed temperature

MD is an evaporative thermal separation process, and the temperature-affected driving force is the vapor partial pressure difference between the feed and permeates sides. As a result, the first element investigated is feed inlet temperature, which is an essential operational parameter.

That has a significant effect on total cross-membrane flux variables due to the thermal-driven separation nature of the MD process. The PVDF flat sheet DCMD system was utilized to examine the effect of feed inlet temperature on total cross-membrane flux for feed inlet temperatures ranging from 313.15 to 358.15 K with a 278.15 K interval. The highest temperature used is lower than the feed solution's boiling point. The permeate inlet temperature, feed inlet NaCl concentration, and flow rate, on the other hand, were held constant. The temperature of the permeate inlet was maintained at 293.15 K, the concentration of NaCl in the feed inlet was maintained at 0.035 kg/kg, and the flow rate on both feed and permeate sides was adjusted at 2 kg/s. Fig. 2 depicts the overall profile of the cross-membrane flux for a variety of feed inlet temperatures.

When the temperature of the feed inlet is raised from 333.15 K to 343.15 K, the total cross-membrane flux increases from 25.6223 kg/(m^2 h) to 39.5313 kg/(m^2 h).

At lower feed inlet temperatures, there was hardly any discernible difference in the overall cross-membrane flux. This is an important point to keep in mind. There is a difference in flux at higher feed inlet temperatures above 343.15 K, with the total cross-membrane flux increasing from 39.5313 kg/(m^2 h) to 68.3627 kg/(m^2 h).

The highest flux generation occurs near the boiling point and low permeate inlet temperature. This significant effect of feed inlet temperature and transmembrane temperature difference on total cross-membrane flux is consistent with previous research [44]. The feed inlet temperature has a strong effect on improving the flux with its increment, as widely accepted in the literature because the flux increases exponentially by increasing the feed inlet temperatures, which causes an increase in water vapor pressure, which is relatively slight at low temperatures but significant at high temperatures, as seen in Antoine's equation by the exponential relationship between saturated vapor pressure and temperature which thus improves the driving force. Although increased feed temperature benefits high flux, energy consumption, and as previously demonstrated by various research [45–47]. Moreover, because of the low effect of temperature polarization in high temperatures, which diminishes with increasing feeding temperature the evaporation temperature is close to the feed bulk temperature, resulting in a large flux.

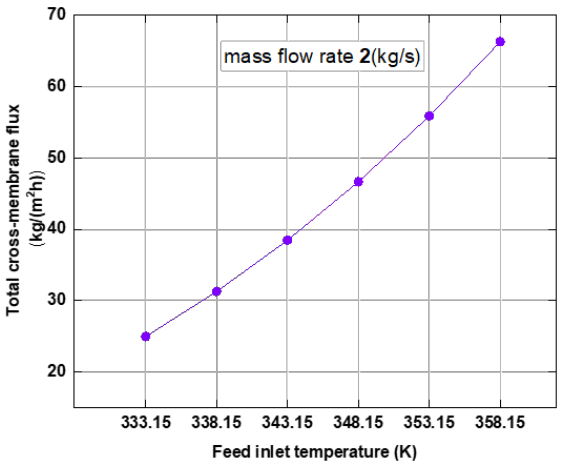

Fig. 2 The total cross-membrane flux as a function of feed side temperature ($T_{p,in}$ = 293.15 K, PVDF membrane)

3.2 Effect of permeate temperature

The effect on the overall improvement of total cross-membrane flux is not confined to the feed inlet temperature alone but also includes the permeate temperature, which has a negligible effect compared to the feeding temperature. A more significant vapor pressure differential at low permeate temperatures resulted in a higher total cross-membrane flux. In most DCMD investigations, the permeate temperature varies between 283.15 to 313.15 K [41].

In this study, the temperature of the permeate inlet ranges anywhere from 288.15 K and 313.15 K. As can be seen in Fig. 3, feed inlet temperatures varied from 328.15 K to 358.15 K with a 278.15 K step under a feed and permeate flow rate of 2 kg/s.

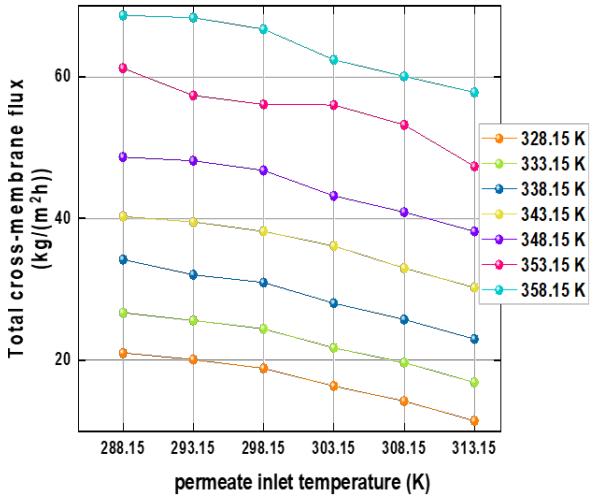

Fig. 3 The effect of permeate inlet temperature on the total cross-membrane flux at different feed inlet temperatures

The curves show that the total cross-membrane flux increases as the permeate temperature decreases, with the highest quantities obtained at the highest temperatures; thus, at 353.15 K and 358.15 K, the total cross-membrane flux rises to 61.2473 and 68.7062 kg/(m^2 h), respectively, at the lowest permeate inlet temperature. This is due the greatest temperatures provide the biggest quantity.

While there is a considerable decrease in total cross-membrane flux as permeate inlet temperature increases, this decline sharply decrease from 288.15 to 313.15 K and due to the decrease in driving force when the temperature difference between the feed and permeate sides decreases.

As a direct result of this, there was not a noticeable improvement in the permeate flux despite the elevation in the permeate inlet temperature. At fixed feed temperatures, the effect of permeate inlet temperature on total cross-membrane flux is almost negligible.

At these temperatures, the only variable of total cross-membrane flux is the water vapor pressure at the permeate-membrane interface (Ppm), which is what causes this weakening effect according to Eq. (1) [48]. This is because the Antoine equation has less fluctuation at lower temperatures, as found by [49, 50].

3.3 Effect of feed and permeate flow rates

The changing hydrodynamic conditions affect the total cross-membrane flux. Permeate flux increases as hydrodynamic conditions increase. Flow rate is the rate at which fluids are debited through the system and has a direct effect on DCMD system performance. The flow rates on both sides of the membrane must be increased to avoid temperature and concentration polarization effects. For each feed inlet temperature condition, a total of four unique feed and permeate flow rates were utilized. These flow rates ranged from 1.0 kg/s to 2.5 kg/s, with a 0.5 kg/s interval between each value. When the temperature at the feed side is increased for each flow rate, trans-membrane flux increases. So, the temperature difference between the two sides of the module may be enlarged, and the total cross-membrane flux is increased, as shown in Fig. 3, and the MD process is enhanced. Fig. 4 shows a noticeable improvement in total cross-membrane flux with higher flow rates.

However, the change that occurred as a result of raising the feed flow rate was rather slight when the feed inlet temperatures were low. It is reliant on the cell on the feed side, which may not be fully flat in shape [51], but there is no noticeable variation across the feed temperature (333.15–343.15 K) at flow rates of 1, 1.5, and 2 kg/s.

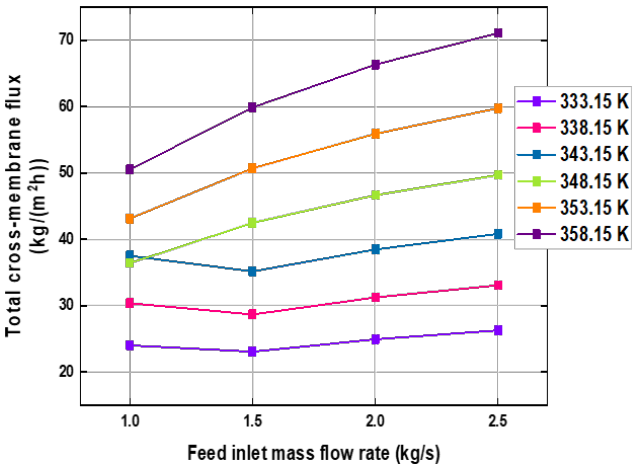

Fig. 4 Total cross-membrane flux as a function of feed and permeate side flow rate at different feed inlet temperatures ($T_{p,in}$ = 293.15 K, PVDF membrane)

In addition, when simulating a flow rate of 2.5 kg/s over a temperature range of (333.15–358.15 K), the total cross-membrane flux acquires the maximum amounts of water vapor at 348.15, 353.15, and 358.15 K, respectively: 50.4980, 61.1611, and 73.2075 kg/(m^2 h). When feed inlet temperatures and flow rates are increased, the resulting flux values are increased as well. When molecules of vapor pass through the membrane from the feed side to the permeate side, the temperature of the surface of the membrane falls below the temperature of the feed bulk.

This results in a boundary layer near the membrane surface, known as a temperature polarization phenomenon. Its influence weakens with increasing flow rate by reducing the thickness of the thermal boundary layer [52]. Overall, the results indicate that a high flux amount was obtained with high flow rates, as clearly shown in Fig. 5.

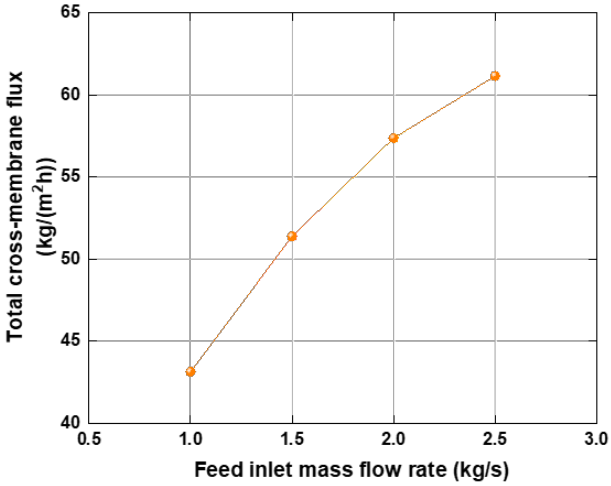

Fig. 5 Overall effect of flow rate variation on the total cross-membrane flux

This behavior is due to the relative thermal boundary layer thickness that gets thinner when the circulation rate increases. Thus, the flux increases due to more effective heat transfer from the bulk to the membrane surface.

3.4 Effect of feed inlet NaCl concentration

To examine the influence of feed inlet NaCl concentration on total cross-membrane flux and the vapor pressure difference that drives the process to create the flux, the objectives of this study are as follows.

The range of feed inlet NaCl concentration that was investigated ranged from 0.035 to 0.285 kg/kg, and all other variables, including flow rate of 2 kg/s, feed inlet side temperature of 358.15 K, permeate side temperature of 293.15 K, were held constant.

The feed inlet NaCl concentrations affect the total cross-membrane flux and the pressure vapor difference; it can change the total cross-membrane flux slightly, especially at lower concentrations, because the flux in the membrane distillation is a function of feed temperature and concentration. As a result, as the feed inlet NaCl concentration increases, the total cross-membrane flux product decreases significantly. The primary reason may be the simultaneous decrease in the vapor pressure difference [50]. In addition, the authors stated that the transition of the solvent from the feed side to the permeate side causes a continuous change in concentration which affects the vapor pressure on the feed side and the thermal conductivity. This behavior proved that the decrease in total cross-membrane flux is related to the low vapor pressure at the feed side, leading to a lower partial pressure gradient between the two sides (decrease in the driving force) [53].

As indicated in Fig. 6, the primary observation is that the total cross-membrane flux reduced when the feed inlet concentration increased on the feed side.

Approximately, when the NaCl concentration increased from 0.035 to 0.335 kg/kg, the total cross-membrane flux decreased by 31.98% from 68.3627 to 46.5031 kg/(m^2 h), and the vapor pressure difference decreased by 13.59% from 11.33 to 9.79 kPa. It is worth noting that increasing the feed inlet NaCl concentration has a more extensive and significant influence on total cross-membrane flux than increasing the vapor pressure difference.

Three phenomena explain this flux decrease: first, temperature polarization [52] is represented by layers formed on both sides of PVDF flat sheet DCMD, second, concentration polarization increased due to the accumulated salt molecules on the membrane surface, which blocked the

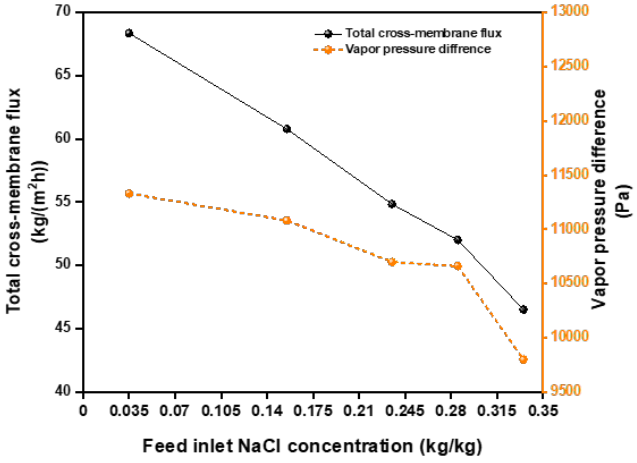

Fig. 6 The effect of NaCl concentration on flux and vapor pressure difference (feed inlet temperature of 358.15 K, permeate inlet temperature of 293.15 K, and flow rate of 2 kg/s)

vapor from moving, resulting in resistance to mass transfer, which causes clogging of pores and increases the risk of scaling the membrane surface [41, 50, 53], which facilitates the membrane pore wetting [54]. Third, fouling reduces the available evaporation area [55, 56] by weakening the membrane's hydrophobicity due to partial wetness and causing the passage of salt molecules through some membrane pores [57]. These factors contribute to a reduction in overall cross-membrane flux generation and quality. Similar findings have been reported by [50, 52–56]. It is worth noting that the effect of temperature and concentration polarization in the MD process decreases when the feed membrane surface temperature is close to the feed bulk temperature [40].

On the other hand, the influence of feed inlet NaCl concentration on total cross-membrane flux was investigated as feed inlet temperature increased.

Fig. 7 shows the curves of results. The feed inlet temperatures ranged from 343.15 to 358.15 K at 278.15 K intervals, with feed inlet concentrations of 0, 0.035, 0.085, and 0.185 kg/kg, and remained constant at 2 kg/s.

However, as feed inlet NaCl concentrations increase from 0 to 0.285 kg/kg at 358.15 K, it drops progressively by 30.17%, from 74.4823 to 52.0099 kg/(m^2 h), bringing the total down to 52.0099 kg/(m^2 h). One more thing to keep in mind is that while the temperature of the feed inlet remains the same, the water activity of the NaCl solution in the feed inlet falls significantly [58, 59] when the amount of NaCl in the feed inlet increases.

This behavior is attributed to adding NaCl in water with concentration [54] because water activity is a function of temperature and NaCl concentration. The same results are shown in Fig. 8, and membranes become less

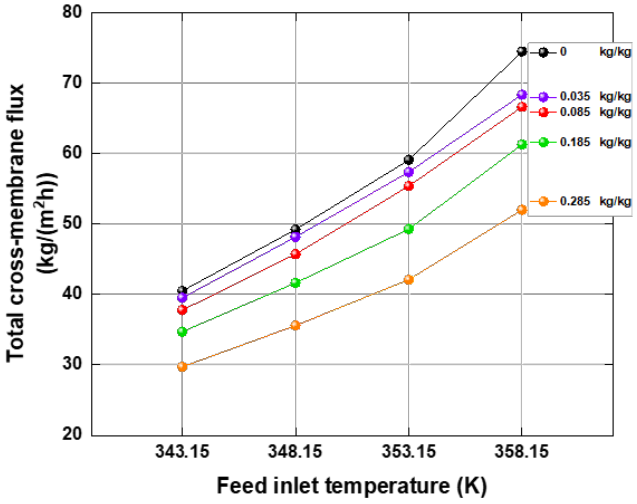

Fig. 7 The effect of feed inlet NaCl concentration on total cross-membrane flux was predicted versus different feed inlet temperatures, at a permeate inlet temperature of 293.15 K, and a flow rate of 2 kg/s

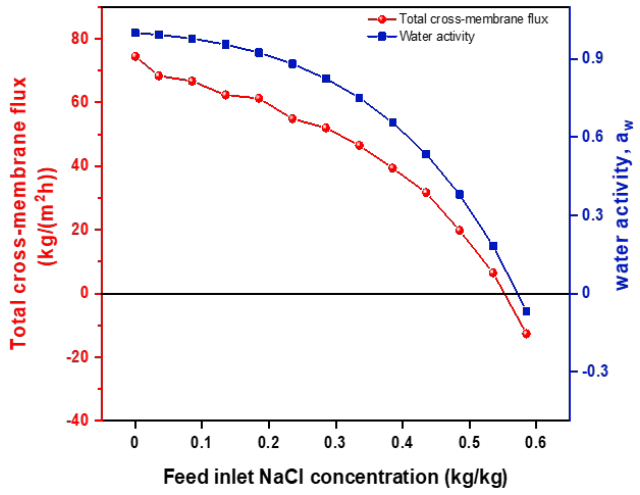

Fig. 9 The effect of water activity on total cross-membrane flux vs. varied feed inlet NaCl concentrations at 358.15 K feed inlet, 293.15 K permeate inlet, and 2 kg/s flow rate

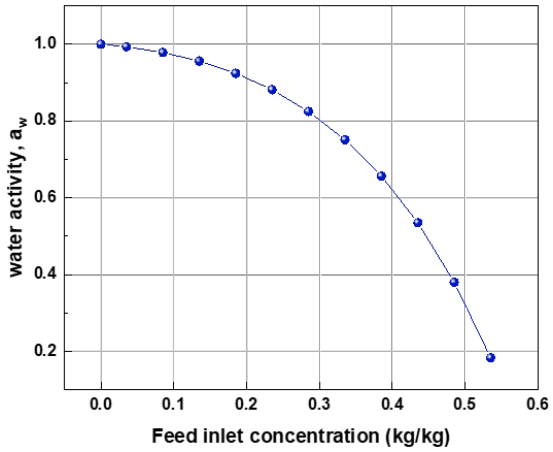

Fig. 8 Water activity predicted different feed inlet NaCl concentrations at a feed inlet temperature of 358.15 K, permeate inlet temperature of 293.15 K, and flow rate of 2 kg/s

conductive. The driving force declines and decreases in total cross-membrane flux [60] until it reaches negative values associated with a rapid fall in water activity [41].

As depicted in Fig. 9, this is the reverse flux phenomenon [54]. Another issue induced by an increase in NaCl concentration at the feed inlet that interrupts evaporation process and affects water quality is the wetting of the membrane pores due to salt deposition on the membrane surface, which accelerates membrane degradation when the water activity level decrease [39].

Water can penetrate the membrane pores as a result of this problem. Membrane wetting refers to membrane pore penetration. To protect the membrane's hydrophobic pores from becoming wet, one of the essential parameters used to describe membrane's hydrophobicity; liquid entry pressure (LEP) must be taken into consideration. This significant character is defined as the minimum hydrostatic pressure required in the liquid feed solution to overcome membrane's hydrophobic forces and allow the liquid to penetrate the membrane pores [39], resulting in the membrane wetting.

Because the feed liquid and any dissolved salts are pushed through the membrane when the liquid entry pressure (LEP) is less than the transmembrane hydrostatic pressure [41]. As a result, to keep away from this phenomenon, the hydrostatic pressure should always be lower than LEP [39]. The LEP is determined by the suitable size and shape of the pore allowing a sufficiently high LEP and the liquid-membrane contact angle.

3.5 Comparison between operating conditions effects: feed temperature, flow rate, permeate temperature, and NaCl concentration

This section compares the effect of feed temperature, permeate temperature, flow rate, and NaCl concentration on the total cross-membrane flux for a co-current PVDF flat. At a flow rate of 2 kg/s on both the feed and permeate sides, the first thing that we are going to do is compare the temperature impacts of the feed and the permeate. A global view of the results is shown in Fig. 10.

This view reveals that the overall cross-membrane flux decreases when the permeate temperature increases while the feed temperature remains the same. Therefore, the total cross-membrane flow decreases by 20.75% when at T_{fin} = 348.15 K in Fig. 10 (a), and the total cross-membrane flux decreases by 16.13% when T_{fin} = 358.15 K in Fig. 10 (b), respectively. As a result, the highest feed inlet and lowest permeate inlet temperatures produced the most extraordinary amounts of the total cross-membrane flux.

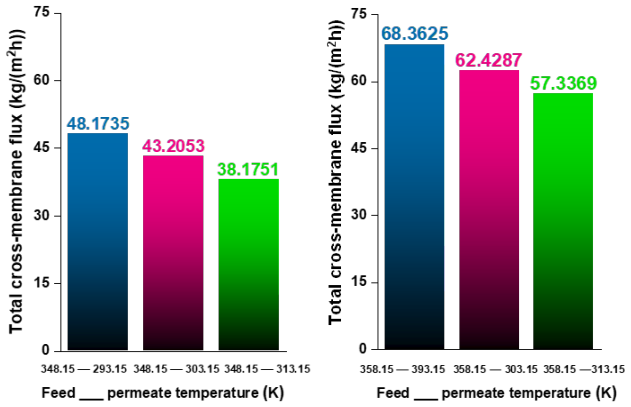

(a) (b)

Fig. 10 Overall fluxes at various temperature combinations ((a) T_{fin} = 348.15 K, (b) T_{fin} = 358.15 K) for a co-current PVDF flat sheet DCMD system with a feed and permeate flow rate of 2 kg/s

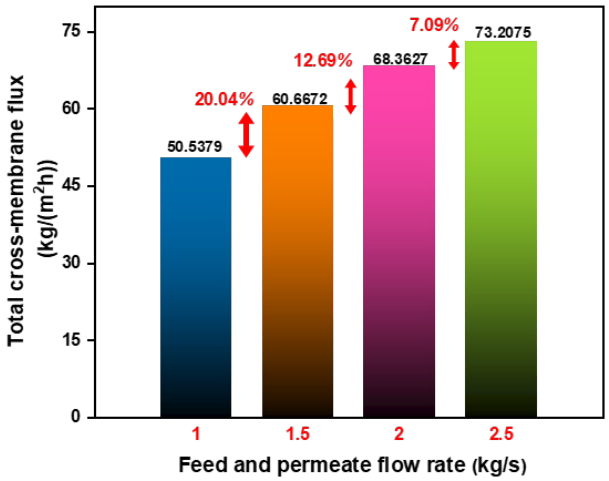

Fig. 12 The effect of flow rates on total cross-membrane flux in a co-current PVDF flat sheet DCMD system with feed and permeate inlet temperatures of 358.15 K and 293.15 K, respectively

Another illustration is presented in Fig. 11; thus, at the same temperature difference (ΔT = 318.15 K) in Fig. 11 (a), the effect of feeding temperature is greater than that of permeation temperature where the flux at the range of (348.15–303.15 K) is compared to that at the temperature of (358.15–313.15 K). This is because the exponential relation between pressure and temperature causes a significant difference in water vapor pressure at higher temperatures. An identical observation can be found in Fig. 11 (b) for the temperature difference (ΔT = 328.15 K).

Second, Fig. 12 depicts the effect of flow rate on the total cross-membrane at a feed inlet temperature of 358.15 K and a permeate inlet temperature of 293.15 K, where the total cross-membrane flux increases by 20.04% between flow rate values of 1 and 1.5 kg/s, 12.69% between 1.5 and 2 kg/s, and 7.09% between 1.5 and 2.5 kg/s and 2 kg/s, and 7.09% between 1.5 and 2.5 kg/s.

Even when the flow rate increases, the ratio of the change in the total cross-membrane flux drops from 12.69 to 7.09%. The effect of flow rate is less pronounced and less influential on the total cross-membrane flux than the influence of temperature, which is more pronounced and effective. Third, make a comparison between the effects of feed temperature and NaCl concentration (Fig. 13).

In comparison, the total cross-membrane flux increases by 64.08% as the feed temperature increases. In comparison to the feed temperature effect, the effect of the feed NaCl concentration is less effective, despite increasing total transmembrane flux when the NaCl concentration decreases. Based on this comparison, it can be concluded

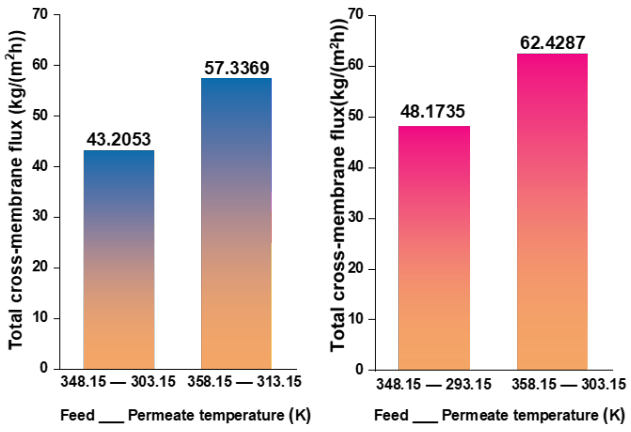

(a) (b)

Fig. 11 Overall fluxes at different temperature differences ((a) ΔT = 318.15 K, (b) ΔT = 328.15 K) for a co-current PVDF flat sheet DCMD system with a flow rate of 2 kg/s for the feed and permeate sides

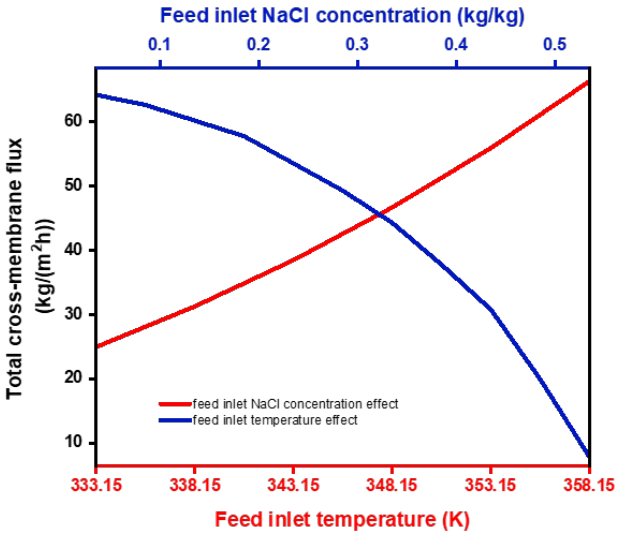

Fig. 13 The feed inlet NaCl concentration effect compared to the feed inlet temperature on the total cross-membrane flux

that the feed inlet temperature has the most significant influence on total cross-membrane flux, as seen in Fig. 14 because of the exponential increase in vapor pressure with temperature, the total cross-membrane flux improvement is more remarkable at higher temperatures.

4 Conclusions

MD transports water vapor through a hydrophobic micro-porous membrane utilizing a thermally-driven separation process to separate hot saline water and cold distillate. MD uses vapor pressure to separate hot saline water and cold distillate into freshwater.

With a micro-porous PVDF flat sheet membrane with 14 (cm^2) area and 0.12 (mm) thickness, several operational factors were theoretically studied on MD process performance (mm). The membrane had a porosity of 0.75, feed inlet temperature (333.15–358.15 K), feed flow rate (1–2.5 kg/s), permeate inlet temperature (288.15–313.15 K), and feed inlet NaCl concentration (0.035–0.485 kg/kg).

Trial-and-error MATLAB-Simulations yielded the results. This last inputs parameter values to construct curves for discussion and analysis. This paper revealed findings about total cross-membrane flux performance:

- The feed inlet temperature affects cross-membrane flux the most, which is beneficial for improvement.
- Flow rate increases cross-membrane flux and decreases the thermal boundary layer.
- Maintaining the permeate inlet temperature at 293.15 K has little effect on total cross-membrane flux, which matches the shift in water vapor pressure and thermal properties (lowest at low temperatures).

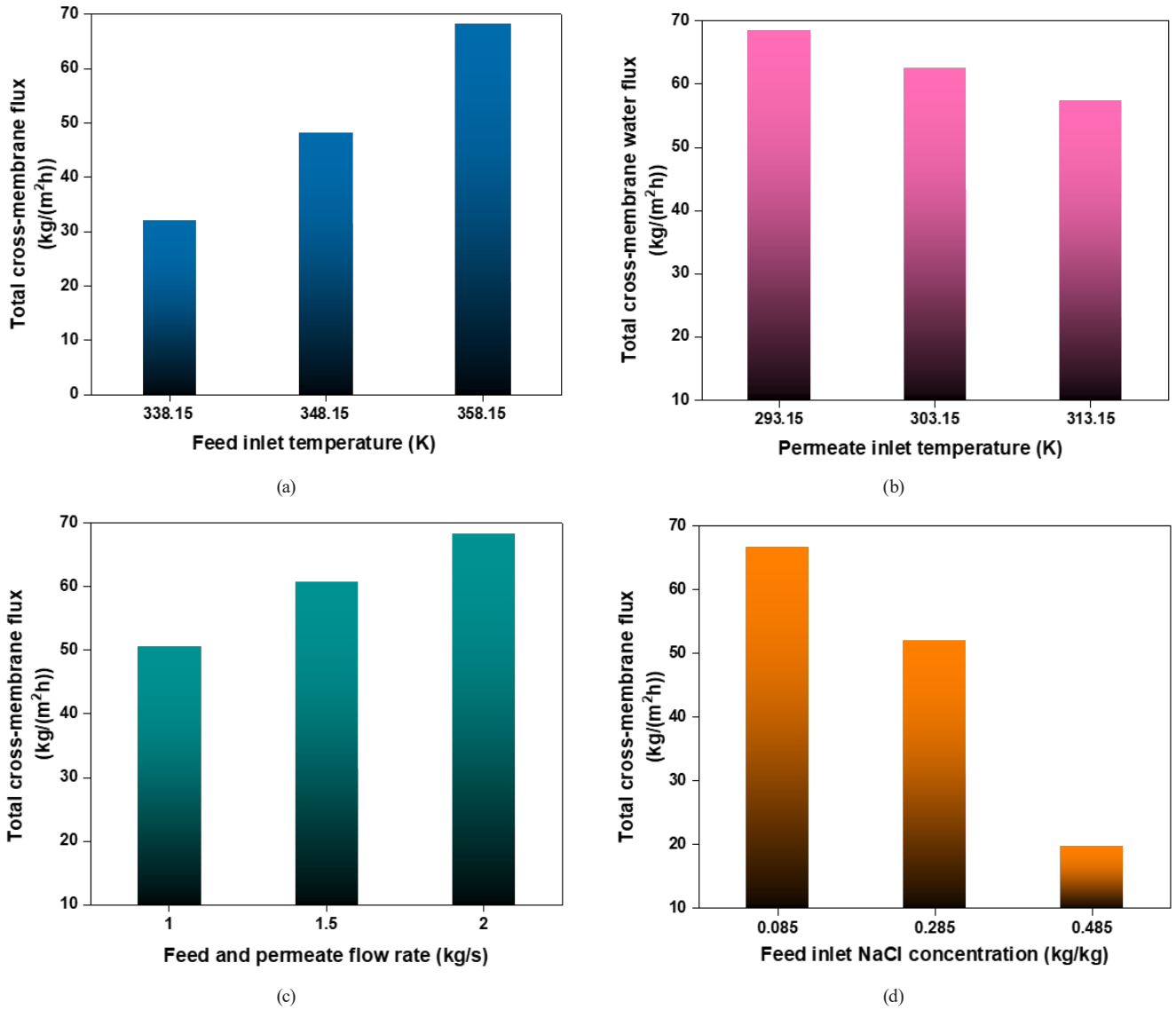

Fig. 14 Comparison of main effects of operating parameters on the total cross-membrane flux: (a) feed inlet temperature, (b) permeate inlet temperature, (c) feed and permeate flow rate, and (d) feed inlet NaCl concentration

- Increased feed inlet NaCl concentration decreased membrane flux and vapor pressure differential, so the feed inlet NaCl concentration's impact on membrane flux was greater than the vapor pressure differential.

This study examined how operating conditions affected membrane flux. The results, which are consistent with previous studies, reveal that feed temperature and flow rate are the most important elements in boosting total cross-membrane flux. The overall cross-membrane flux increases with increasing feed inlet temperature and flow rate and decreases with increasing permeate inlet temperature and NaCl concentration.

At 358.15 K feed inlet temperature, 293.15 K permeate inlet temperature, 2.5 kg/s flow rate, and 0.035 kg/kg feed inlet NaCl concentration, PVDF flat sheet membranes produce 73.2075 kg/(m^2 h) total cross-membrane flux.

PVDF flat-sheet membranes provide a significantly higher total cross-membrane flux at higher feed inlet temperatures. This confirms that membranes can handle higher temperatures.

References

[1] Obotey Ezugbe, E., Rathilal, S. "Membrane technologies in wastewater treatment: A review", Membranes, 10(5), 89, 2020. https://doi.org/10.3390/membranes10050089

[2] Siddiqi, M. M., Naseer, M. N. "A sustainable integrated water and energy production plan to meet future requirements-A case study of Pakistan", Journal of Research in Environmental Science and Toxicology, 8(1), pp. 38–45, 2019. https://doi.org/10.14303/jrest.2018.022

[3] Taloba, A. I. "An artificial neural network mechanism for optimizing the water treatment process and desalination process", Alexandria Engineering Journal, 61(12), pp. 9287–9295, 2022. https://doi.org/10.1016/j.aej.2022.03.029

[4] Hailemariam, R. H., Woo, Y. C., Damtie, M. M., Kim, B. C., Park, K.-D., Choi, J.-S. "Reverse osmosis membrane fabrication and modification technologies and future trends: A review", Advances in Colloid and Interface Science, 276, 102100, 2020. https://doi.org/10.1016/j.cis.2019.102100

[5] Moslehyani, A., Ismail, A. F., Matsuura, T., Rahman, M. A., Goh, P. S. "Chapter 3 - Recent progresses of ultrafiltration (UF) membranes and processes in water treatment", In: Ismail, A. F., Rahman, M. A., Othman, M. H. D., Matsuura, T. (eds.) Membrane Separation Principles and Applications: From Materials Selection to Mechanisms and Industrial Uses, Elsevier, 2019, pp. 85–110. ISBN 978-0-12-812815-2 https://doi.org/10.1016/B978-0-12-812815-2.00003-X

[6] Yu, H., Li, X., Chang, H., Zhou, Z., Zhang, T., Yang, Y., Li, G., Ji, H., Cai, C., Liang, H. "Performance of hollow fiber ultrafiltration membrane in a full-scale drinking water treatment plant in China: A systematic evaluation during 7-year operation", Journal of Membrane Science, 613, 118469, 2020. https://doi.org/10.1016/j.memsci.2020.118469

[7] Zhao, C., Ge, R., Zhen, Y., Wang, Y., Li, Z., Shi, Y., Chen, X. "A hybrid process of coprecipitation-induced crystallization-capacitive deionization-ion exchange process for heavy metals removal from hypersaline ternary precursor wastewater", Chemical Engineering Journal, 378, 122136, 2019. https://doi.org/10.1016/j.cej.2019.122136

[8] Rathi, B. S., Kumar, P. S. "Electrodeionization theory, mechanism and environmental applications. A review", Environmental Chemistry Letters, 18(4), pp. 1209–1227, 2020. https://doi.org/10.1007/s10311-020-01006-9

[9] Iwuozor, K. O. "Prospects and challenges of using coagulation-flocculation method in the treatment of effluents", Advanced Journal of Chemistry-Section A, 2(2), pp. 105–127, 2019. https://doi.org/10.29088/SAMI/AJCA.2019.2.105127

[10] Xing, J., Liang, H., Xu, S., Chuah, C. J., Luo, X., Wang, T., Wang, J., Li, G., Snyder, S. A. "Organic matter removal and membrane fouling mitigation during algae-rich surface water treatment by powdered activated carbon adsorption pretreatment: Enhanced by UV and UV/chlorine oxidation", Water Research, 159, pp. 283–293, 2019. https://doi.org/10.1016/j.watres.2019.05.017

[11] dos Santos, P. R., Daniel, L. A. "A review: organic matter and ammonia removal by biological activated carbon filtration for water and wastewater treatment", International Journal of Environmental Science and Technology, 17(1), pp. 591–606, 2020. https://doi.org/10.1007/s13762-019-02567-1

[12] Srivastav, A. L., Patel, N., Chaudhary, V. K. "Disinfection by-products in drinking water: Occurrence, toxicity and abatement", Environmental Pollution, 267, 115474, 2020. https://doi.org/10.1016/j.envpol.2020.115474

[13] Lim, S., Shi, J. L., von Gunten, U., McCurry, D. L. "Ozonation of organic compounds in water and wastewater: A critical review", Water Research, 213, 118053, 2022. https://doi.org/10.1016/j.watres.2022.118053

[14] Ghaffour, N., Soukane, S., Lee, J.-G., Kim, Y., Alpatova, A. "Membrane distillation hybrids for water production and energy efficiency enhancement: A critical review", Applied Energy, 254, 113698, 2019. https://doi.org/10.1016/j.apenergy.2019.113698

[15] Zare, S., Kargari, A. "4 - Membrane properties in membrane distillation", In: Gude, V. G. (ed.) Emerging Technologies for Sustainable Desalination Handbook, Butterworth-Heinemann, 2018, pp. 107–156. ISBN 978-0-12-815818-0 https://doi.org/10.1016/B978-0-12-815818-0.00004-7

[16] Parani, S., Oluwafemi, O. S. "Membrane distillation: Recent configurations, membrane surface engineering, and applications", Membranes, 11(12), 934, 2021. https://doi.org/10.3390/membranes11120934

[17] Jose, A. J., Kappen, J., Alagar, M. "2 - Polymeric membranes: Classification, preparation, structure physiochemical, and transport mechanisms", In: Thomas, S., Balakrishnan, P., Sreekala, M. S. (eds.) Fundamental Biomaterials: Polymers, Woodhead Publishing, 2018, pp. 21–35. ISBN 978-0-08-102194-1 https://doi.org/10.1016/B978-0-08-102194-1.00002-5

[18] Khan, E. U., Nordberg, Å. "Thermal integration of membrane distillation in an anaerobic digestion biogas plant – A techno-economic assessment", Applied Energy, 239, pp. 1163–1174, 2019. https://doi.org/10.1016/j.apenergy.2019.02.023

[19] Ochando-Pulido, J. M., Stoller, M., Di Palma, L., Martínez-Ferez, A. "On the optimization of a flocculation process as fouling inhibiting pretreatment on an ultrafiltration membrane during olive mill effluents treatment", Desalination, 393, pp. 151–158, 2016. https://doi.org/10.1016/j.desal.2015.12.021

[20] Ni, W., Li, Y., Zhao, J., Zhang, G., Du, X., Dong, Y. "Simulation study on direct contact membrane distillation modules for high-concentration NaCl solution", Membranes, 10(8), 179, 2020. https://doi.org/10.3390/membranes10080179

[21] Choi, J., Cho, J., Shin, J., Cha, H., Jung, J., Song, K. G. "Performance and economic analysis of a solar membrane distillation pilot plant under various operating conditions", Energy Conversion and Management, 268, 115991, 2022. https://doi.org/10.1016/j.enconman.2022.115991

[22] Chang, H., Ho, C.-D., Chen, Y.-H., Chen, L., Hsu, T.-H., Lim, J.-W., Chiou, C.-P., Lin, P.-H. "Enhancing the Permeate Flux of Direct Contact Membrane distillation modules with inserting 3D printing turbulence promoters", Membranes, 11(4), 266, 2021. https://doi.org/10.3390/membranes11040266

[23] Francis, L., Ahmed, F. E., Hilal, N. "Advances in Membrane Distillation Module Configurations", Membranes, 12(1), 81, 2022. https://doi.org/10.3390/membranes12010081

[24] Suárez, F., del Río, M. B., Aravena, J. E. "Water Flux Prediction in Direct Contact Membrane Distillation Subject to Inorganic Fouling", Membranes, 12(2), 157, 2022. https://doi.org/10.3390/membranes12020157

[25] Hidayah, M., Kusworo, T. D., Susanto, H. "Improving the Performance of Polysulfone-nano ZnO Membranes for Water Treatment in Oil Refinery with Modified UV Irradiation and Polyvinyl Alcohol", Periodica Polytechnica Chemical Engineering, 66(1), pp. 43–53, 2022. https://doi.org/10.3311/PPch.17029

[26] Khalifa, A., Ahmad, H., Antar, M., Laoui, T., Khayet, M. "Experimental and theoretical investigations on water desalination using direct contact membrane distillation", Desalination, 404, pp. 22–34, 2017. https://doi.org/10.1016/j.desal.2016.10.009

[27] Alwatban, A. M., Alshwairekh, A. M., Alqsair, U. F., Alghafis, A. A., Oztekin, A. "Effect of membrane properties and operational parameters on systems for seawater desalination using computational fluid dynamics simulations", Desalination and Water Treatment, 161, pp. 92–107, 2019. https://doi.org/10.5004/dwt.2019.24275

[28] Laqbaqbi, M., García-Payo, M. C., Khayet, M., El Kharraz, J., Chaouch, M. "Application of direct contact membrane distillation for textile wastewater treatment and fouling study", Separation and Purification Technology, 209, pp. 815–825, 2019. https://doi.org/10.1016/j.seppur.2018.09.031

[29] Al-Salmi, M., Laqbaqbi, M., Al-Obaidani, S., Al-Maamari, R. S., Khayet, M., Al-Abri, M. "Application of membrane distillation for the treatment of oil field produced water", Desalination, 494, 114678, 2020. https://doi.org/10.1016/j.desal.2020.114678

[30] Li, J., Ren, L.-F., Zhou, H. S., Yang, J., Shao, J., He, Y. "Fabrication of superhydrophobic PDTS-ZnO-PVDF membrane and its anti-wetting analysis in direct contact membrane distillation (DCMD) applications", Journal of Membrane Science, 620, 118924, 2021. https://doi.org/10.1016/j.memsci.2020.118924

[31] Foureaux, A. F. S., Moreira, V. R., Lebron, Y. A. R., de Souza Santos, L. V., Amaral, M. C. S. "A sustainable solution for fresh-water demand in mining sectors: Process water reclamation from POX effluent by membrane distillation", Separation and Purification Technology, 256, 117797, 2021. https://doi.org/10.1016/j.seppur.2020.117797

[32] Wanke, D., da Silva, A., Costa, C. "Modification of PVDF hydrophobic microfiltration membrane with a layer of electrospun fibers of PVP-*co*-PMMA: Increased fouling resistance", Chemical Engineering Research and Design, 171, pp. 268–276, 2021. https://doi.org/10.1016/j.cherd.2021.05.004

[33] Niknejad, A. S., Bazgir, S., Kargari, A. "Desalination by direct contact membrane distillation using a superhydrophobic nanofibrous poly (methyl methacrylate) membrane", Desalination, 511, 115108, 2021. https://doi.org/10.1016/j.desal.2021.115108

[34] Bin Bandar, K., Alsubei, M. D., Aljlil, S. A., Bin Darwish, N., Hilal, N. "Membrane distillation process application using a novel ceramic membrane for Brackish water desalination", Desalination, 500, 114906, 2021. https://doi.org/10.1016/j.desal.2020.114906

[35] Fortunato, L., Elcik, H., Blankert, B., Ghaffour, N., Vrouwenvelder, J. "Textile dye wastewater treatment by direct contact membrane distillation: Membrane performance and detailed fouling analysis", Journal of Membrane Science, 636, 119552, 2021. https://doi.org/10.1016/j.memsci.2021.119552

[36] de Sousa Silva, R., Cavalcanti, C. D. Á. K., de Cassia Siqueira Curto Valle, R., Francisco Machado, R. A., Marangoni, C. "Understanding the effects of operational conditions on the membrane distillation process applied to the recovery of water from textile effluents", Process Safety and Environmental Protection, 145, pp. 285–292, 2021. https://doi.org/10.1016/j.psep.2020.08.022

[37] Dong, G., Kim, J. F., Kim, J. H., Drioli, E., Lee, Y. M. "Open-source predictive simulators for scale-up of direct contact membrane distillation modules for seawater desalination", Desalination, 402, pp. 72–87, 2017. https://doi.org/10.1016/j.desal.2016.08.025

[38] Lawson, K. W., Lloyd, D. R. "Membrane distillation", Journal of Membrane Science, 124(1), pp. 1–25, 1997. https://doi.org/10.1016/S0376-7388(96)00236-0

[39] Alkhudhiri, A., Hilal, N. "3 - Membrane Distillation—Principles, applications, configurations, design, and implementation", In: Gude, V. G. (ed.) Emerging Technologies for Sustainable Desalination Handbook, Butterworth-Heinemann, 2018, pp. 55–106. ISBN 978-0-12-815818-0 https://doi.org/10.1016/B978-0-12-815818-0.00003-5

[40] Yun, Y., Ma, R., Zhang, W., Fane, A. G., Li, J. "Direct contact membrane distillation mechanism for high concentration NaCl solutions", Desalination, 188(1–3), pp. 251–262, 2006. https://doi.org/10.1016/j.desal.2005.04.123

[41] Khayet, M., Matsuura, T. "Chapter 10 – Direct Contact Membrane Distillation", In: Membrane Distillation: Principles and Applications, Elsevier, 2011, pp. 249–293. ISBN 978-0-444-53126-1 https://doi.org/10.1016/B978-0-444-53126-1.10010-7

[42] Alkhudhiri, A., Darwish, N., Hilal, N. "Membrane distillation: A comprehensive review", Desalination, 287, pp. 2–18, 2012. https://doi.org/10.1016/j.desal.2011.08.027

[43] Essalhi, M., Khayet, M. "Self-sustained webs of polyvinylidene fluoride electrospun nanofibers at different electrospinning times: 2. Theoretical analysis, polarization effects and thermal efficiency", Journal of Membrane Science, 433, pp. 180–191, 2013. https://doi.org/10.1016/j.memsci.2013.01.024

[44] Anvari, A., Kekre, K. M., Azimi Yancheshme, A., Yao, Y., Ronen, A. "Membrane distillation of high salinity water by induction heated thermally conducting membranes", Journal of Membrane Science, 589, 117253, 2019. https://doi.org/10.1016/j.memsci.2019.117253

[45] Qtaishat M, Matsuura T, Kruczek B, Khayet M. "Heat and mass transfer analysis in direct contact membrane distillation", Desalination, 219(1–3), pp. 272–292, 2008. https://doi.org/10.1016/j.desal.2007.05.019

[46] Song, Z., Li, L., Wang, H., Li, B., Wang, S. "DCMD flux curve characteristics of cross-flow hollow fiber membrane", Desalination, 323, pp. 107–113, 2013. https://doi.org/10.1016/j.desal.2012.05.005

[47] Cath, T. Y., Adams, D. A., Childress, A. E. "Experimental study of desalination using direct contact membrane distillation: a new approach to flux enhancement", Journal of Membrane Science, 228(1), pp. 5–16, 2004. https://doi.org/10.1016/j.memsci.2003.09.006

[48] Cai, J., Guo, F. "Study of mass transfer coefficient in membrane desalination", Desalination, 407, pp. 46–51, 2017. https://doi.org/10.1016/j.desal.2016.12.013

[49] Matheswaran, M., Kwon, T. O., Kim, J. W., Moon, I. S. "Factors affecting flux and water separation performance in air gap membrane distillation", Journal of Industrial and Engineering Chemistry, 13(6), pp. 965–970, 2007.

[50] Alkhudhiri, A., Hilal, N. "Air gap membrane distillation: A detailed study of high saline solution", Desalination, 403, pp. 179–186, 2017. https://doi.org/10.1016/j.desal.2016.07.046

[51] Singh, D., Sirkar, K. K. "Desalination of brine and produced water by direct contact membrane distillation at high temperatures and pressures", Journal of Membrane Science, 389, pp. 380–388, 2012. https://doi.org/10.1016/j.memsci.2011.11.003

[52] Tomaszewska, M. "Temperature polarization", In: Drioli, E., Giorno, L. (eds.) Encyclopedia of membranes, Springer, 2016, pp. 1879–1880. ISBN 978-3-662-44323-1 https://doi.org/10.1007/978-3-662-44324-8_573

[53] Ali, A. "Evaluation of membrane characteristics and thermal polarization in membrane distillation", PhD Thesis, Université Paul Sabatier-Toulouse III, 2015.

[54] Guan, Y., Li, J., Cheng, F., Zhao, J., Wang, X. "Influence of salt concentration on DCMD performance for treatment of highly concentrated NaCl, KCl, $MgCl_2$ and $MgSO_4$ solutions", Desalination, 355, pp. 110–117, 2015. https://doi.org/10.1016/j.desal.2014.10.005

[55] Choudhury, M. R., Anwar, N., Jassby, D., Rahaman, M. S. "Fouling and wetting in the membrane distillation driven wastewater reclamation process – A review", Advances in Colloid and Interface Science, 269, pp. 370–399, 2019. https://doi.org/10.1016/j.cis.2019.04.008

[56] Drioli, E., Ali, A., Macedonio, F. "Membrane distillation: Recent developments and perspectives", Desalination, 356, pp. 56–84, 2015. https://doi.org/10.1016/j.desal.2014.10.028

[57] El-Bourawi, M. S., Ding, Z., Ma, R., Khayet, M. "A framework for better understanding membrane distillation separation process", Journal of Membrane Science, 285(1–2), pp. 4–29, 2006. https://doi.org/10.1016/j.memsci.2006.08.002

[58] Xu, J., Singh, Y. B., Amy, G. L., Ghaffour, N. "Effect of operating parameters and membrane characteristics on air gap membrane distillation performance for the treatment of highly saline water", Journal of Membrane Science, 512, pp. 73–82, 2016. https://doi.org/10.1016/j.memsci.2016.04.010

[59] Martínez, L. "Comparison of membrane distillation performance using different feeds", Desalination, 168, pp. 359–365, 2004. https://doi.org/10.1016/j.desal.2004.07.022

[60] Martínez, L., Rodríguez-Maroto, J. M. "On transport resistances in direct contact membrane distillation", Journal of Membrane Science, 295(1–2), pp. 28–39, 2007. https://doi.org/10.1016/j.memsci.2007.02.029